Microwave-assisted ammonia decomposition reaction over iron incorporated mesoporous carbon catalysts

Dilek Varisli [a,*], Cansu Korkusuz [b], Timur Dogu [c]

[a] Advanced Technologies, Graduate School of Natural and Applied Sciences, Gazi University, 06500, Ankara, Turkey
[b] Department of Chemical Engineering, Gazi University, 06500, Ankara, Turkey
[c] Department of Chemical Engineering, Middle East Technical University, 06800, Ankara, Turkey

ABSTRACT

Microwave-assisted ammonia decomposition reaction was investigated to produce CO_x free hydrogen, for fuel cell applications. Iron incorporated mesoporous carbon catalysts were prepared at different metal loadings, following an impregnation procedure. Mesoporous carbon acted as the catalyst support, as well as the microwave receptor. Complete conversion of ammonia was achieved at 450 °C over the catalyst having 7.7 wt% Fe, when the reaction was carried out in the microwave reactor system, using pure ammonia (GHSV of 36000 ml/h g_{cat}). However, in the case of using the conventionally heated reactor, complete conversion of ammonia was achieved only at 600 °C. Iron oxides, namely maghemite (γ-Fe_2O_3), magnetite (Fe_3O_4) and hematite (α-Fe_2O_3) simultaneously appeared in the structure of the synthesized catalysts, after their calcination at 450 °C, under pure N_2 flow. Iron oxides present in the calcined catalytic materials then were reduced to metallic iron at 500 °C. Formation of iron carbide crystals was observed in the structure of spent catalysts that were used in microwave reactor system, while metallic iron crystals were still present in the catalysts that were tested in conventionally heated system.

© 2016 Elsevier B.V. All rights reserved.

1. Introduction

In recent years, ammonia has been considered as an important raw material for hydrogen production, since conventional routes, such as steam reforming, result in formation of COx components besides hydrogen. These byproducts cause a decrease in fuel cell performance due to their poisoning effect [1,2]. Sources of ammonia can be either in liquid or solid form. Generally known, ammonia is a valuable chemical that can be commonly used in different industrial processes to produce fertilizers, animal feed and to manufacture explosives, paper, rubber etc [3]. At ambient temperature and pressure, ammonia is present in gaseous form. It can be easily liquefied at 298 K under the pressure of about 10 bar and can be stored in relatively inexpensive pressure vessels [4]. However, under ambient conditions it has malodorus and it is harmfull and may damage human health and environments [3]. During the production of ammonia and urea, excessive amount of ammonia is being emitted to the atmosphere or discharged with wastewater effluent streams which cause water pollution problem as well as loss of raw materials. It should be pointed out that acceptable ammonia and urea level for wastewater of urea plants should be lower than 10 ppm for both of them. So removal and recovery of ammonia from wastewater is important [5,6]. Different methods such as biological processes, ion exchange, micro-wave plasma discharge, water scrubbing, air stripping, electrochemical oxidation have been applied for the treatment of ammonia removal. These kind of processes generally involve a phase transformation and result in contaminated sludge. Therefore adsorbent require further disposal and their maintenance and operation are costly [7,3]. Recently decomposition reaction has been proposed to decrease ammonia concentration in waste water since it produces COx free hydrogen which is one of the highly promising alternative energy sources [5,3].

Ammonia decomposition reaction has been studied using a number of catalysts. Ruthenium is known to be the most active metal among single metals and various studies have been carried out using ruthenium with different supports [8–12]. In order to commercialize the production of COx free hydrogen production from ammonia, studies on the preparation of highly active catalysts using much cheaper metals, such as Ni [2,13,14], Fe [9,13,15–17], Co [18,19] have been performed by different research groups.

Microwaves are present between infrared radiation and radiowaves in the electromagnetic spectrum. They have wavelengths between 0.001 and 1 m and the corresponding frequencies

are between 300 and 0.3 GHz. They are generally used in telecommunications and radar transmissions. In domestic microwave ovens, which are used for food processing and industrial microwave applications for chemical synthesis, a microwave frequency value of about 2.45 GHz is used, in order to avoid any interference with telecommunication microwaves [20,21]. Nowadays, microwave energy is used as an alternative heating method to enhance heterogenous chemical reactions, for either endothermic or exothermic ones. Unlikely conventional heating methods, heat is generated by direct conversion of electromagnetic energy [22,23]. Indeed, the interaction of charged particles in a material with the electric field component of electromagnetic radiation, i.e. microwave frequency waves, resulted in the material to heat up [20]. So, heating from interior of the material occurs [22,23] and better energy utilization is obtained [24]. Since selective, volumetric, uniform and non-contact heating occur in microwave focused reaction systems, rate enhancement, higher yields and improved selectivities can be obtained [22,23,25–27]. Lower coke formation and highly stable performance during the reaction were also reported for microwave systems [24]. Less time is required for heating in the reaction medium [28]. Unlike the conventional systems, less energy input for heating was also discussed in the literature [29]. Other advantages of using microwave heating system are (i) a greater control of heating process, (ii) quick start and stop facility, (iii) high level of safety and automation and (iv) reduced equipment [22,23,28]. Microwave heating has been applied in a variety of chemical reactions, such as pyrolysis of coffee hulls to hydrogen rich fuel gas [28], CO_2 free hydrogen production by methane decomposition [22], pyrolysis of methane to hydrogen [30], growth of nanofilament from methane [26], dry reforming of methane [31], biodiesel production from soybean oil [29], methanol autothermal reforming [32], steam gasification of process of biochar [25], steam reforming of ethanol [27], and methanol [33], water gas shift reaction [34], pyrolysis of coal [35] and pyrolysis of rice straw for hydrogen production [36]. Although different studies are reported for hydrogen production, an application of microwave reactors for the ammonia decomposition reaction is missing in the literature.

In order to absorb microwave energy, a dielectric material should be used in the reactor system [24]. However, not all of the materials have the ability to absorb microwave. Dielectric loss tangent is used for explaining the ability of a material to be heated in the presence of microwave and it is calculated using dielectric constant, i.e., a measure of how much incident energy is absorbed and dielectric loss factor, i.e., a measure of dissipiation of electric energy in the form of heat [20]. Carbonaceous materials are known as strong absorbers of microwave, considering their dielectric loss tangent values. They have the ability of converting microwave energy to thermal energy which results in an increase in temperature [31,20,35]. When carbonaceous materials are used as a catalyst in a reaction medium, they act not only as a catalyst but also as a microwave receptor in this medium [31]. If the catalyst is transparent to microwave, carbonaceous material is used as a receptor together with the catalyst to enhance the reaction [20].

In the present study mesoporous carbon is selected as the carbonaceous material which will act as a catalyst support and also a microwave receptor and iron is used as the active component of the catalyst for ammonia decomposition reaction. Different studies on iron incorporated mesoporous carbon catalysts have been reported for different reactions, due to the superior properties of mesoporous carbon, such as high chemical stability, good thermal conductivity, weak metal-carbon interaction, large pore size and uniform pore structure [37–40]. Minchev et al. [37] prepared iron oxide modified CMK-n type mesoporous carbon catalysts by wet impregnation procedure and used in methanol decomposition reaction. Li et al. [38] prepared Fe-containing mesoporous carbon materials following a soft templating route and tested in the cat-

alytic wet peroxide oxidation of phenol. Duan et al. [39] prepared ordered mesoporous carbon supported iron catalysts by an incipient wetness impregnation procedure to be used in Fenton-like degradation of 4-chlorophenol. Cruz et al. [40] synthesized iron based polymeric mesoporous catalysts for Fischer-Tropsch synthesis using wet impregnation procedure. An application of iron incorporated mesoporous carbon catalysts for ammonia decomposition reaction is limited in the literature. Lu and coworkers [15] prepared γ-Fe_2O_3 supported on CMK-5 which was a bimodal mesoporous ordered carbon by impregnation procedure. They reported complete conversion of ammonia at 700 °C and space velocity of 60000 cm^3/h g$_{cat}$ over these catalysts in the conventional system.

In the present study hydrogen production from ammonia was investigated in a focused microwave heated system over the iron incorporated mesoporous carbon catalysts and the results were compared with the corresponding results obtained in a conventionally heated tubular reactor.

2. Experimental

2.1. Catalyst preparation

Iron incorporated mesoporous carbon catalysts were prepared following an impregnation procedure. Commercially available mesoporous carbon (99.95% purity, Sigma Aldrich) was used as a support material. It was selected due to its ability to act as a microwave receptor in converting electromagnetic energy into heat. Iron nitrate (Fe(NO$_3$)$_3$9H$_2$O, Sigma Aldrich) was used as a metal precursor and catalysts were prepared adjusting Fe wt% in the synthesis solution being between 5 and 15. A mixture was prepared solving 0.5 g of carbon source in a 5 ml of ethanol solution (vol 20%). Then, ethanol solution of iron precursor was added into this mixture in a dropwise manner. The final solution was stirred at 60 °C with a rate of 280 rpm for 3 h and then it was kept at 80 °C for 10 h, until complete drying. Finally, the obtained sample was calcined under the flow of nitrogen (60 ml/min) at 450 °C for 5 h. Catalysts were called as Fe@MC(X), where X referred to the weight% of Fe to the mixture of Fe and mesoporous carbon, in the preparation of synthesis solution. Calcined catalysts were reduced just before each experiment under the flow of pure hydrogen at 500 °C.

2.2. Catalyst characterization

Different techniques were applied in order to characterize the synthesized catalysts. Thermal analysis (TGA-DTA) was performed using Perkin Elmer Pyris 1 Instrument, with a heating rate of 20 °C/min, under the flow of nitrogen, with a flow rate of 100 ml/min. It was used to determine the appropriate temperature for calcination process. Temperature programme reduction (TPR) experiments were carried out using Chembet–3000 instrument. Prior to the analysis, the sample was firstly degassed at 150 °C under the flow of pure He during 1 h, and then cooled to room temperature. Reduction was performed from room temperature to 800 °C under the flow of %5 H$_2$ in nitrogen. Inductively coupled plasma (ICP) analyses were carried out by Perkin Elmer DRC II model ICP-OES equipment to measure the exact metal content of the synthesized catalysts. Nitrogen adsorption-desorption analyses were carried out at 77 K, using the Quantachrome Autosorb–6B instrument, after the samples were degassed at 200 °C for 3 h. The surface area was calculated using the Brunauer, Emmett and Teller (BET) method and pore size distributions were calculated by applying the BJH method to the desorption isotherm. Powder X-Ray diffraction (XRD) analyses were performed by a BRUKER-AXS D8 ADVANCE A 25 diffractometer with a Cu Kα radiation source, operated at 40 kV voltages and 40 mA current. The diffractograms
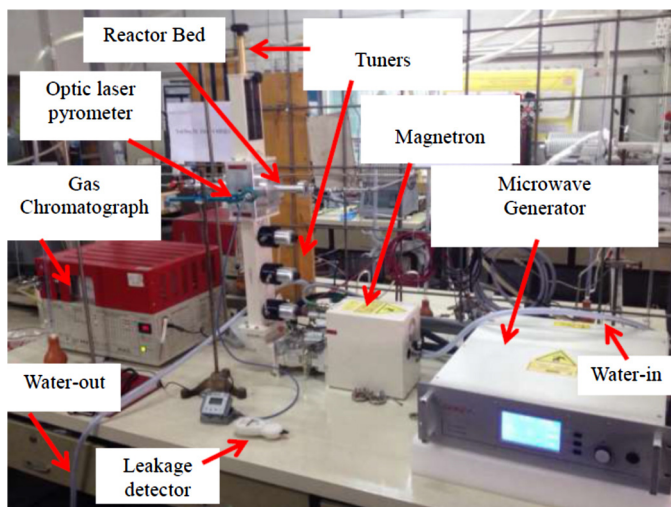
Fig. 1. Microwave Reactor System.

Fig. 2. TGA/DTA result of iron incorporated mesoporous carbon catalyst.

were recorded in the range 5–90° with steps of 0.02°. Average crystallite sizes were calculated by Scherrer formula, which was $D = (K^* \lambda)/(\beta^* \cos\theta)$, where $K = 0.89$, $\lambda = 0.154056$ nm, β was the full width at half maximum of diffraction peaks and θ was the Bragg angle. The diffractograms were compared with of Joint Committee of Diffraction Data (JCPDS) and International Centre for Diffraction Data (ICDD) database. The texture and porosity of the synthesized catalysts were determined by JEOL JEM 2100F high resolution transmission electron microscope (HRTEM) with a maximum acceleration voltage of 200 kV. Each sample was dispersed in ethanol and one drop of this suspension was deposited on a grid covered by C-film to carry out analysis.

2.3. Catalytic performance of the catalysts in different heating systems

Catalytic performances of the synthesized catalysts were tested using two different systems (reactors) having different heat sources. In one of these systems, necessary heat for the reaction was supplied with an electrical furnace (tubular reactor) and it was called as Conventional System (C). A fixed bed quartz tubular reactor having an inner diameter of 13 mm was placed in a temperature controlled tubular electrical furnace and the reaction temperature was changed from 400 to 600 °C. In the second system, which was called as Microwave System (M), reaction was performed in a focused microwave reactor, supplied by SAIREM Company, with a maximum working power of 2 KW and a frequency of 2.45 GHz (Fig. 1). Quartz reactors used in conventional heating system were also utilized in the microwave system. It should be noted that quartz reactors are transparent to microwaves [27]. For both of the system, 0.1 g of reduced catalyst was placed in the middle of the quartz tube and it was supported from both ends. This catalytic bed portion occupied a volume with a length of 12 mm. Unlike Conventional System, microwave power was directly focused to this catalytic bed portion to increase the reaction temperature. Indeed, the reaction temperature was adjusted by changing the power source in microwave system and measured by using an infrared pyrometer (Raytek M13) which was placed at a location looking directly to the catalytic bed. Initially, generator power was set to 0.06 kW and it was gradually increased to 0.09 kW to obtain higher temperatures. It should be noted that, for each of the catalyst the same generator power was set to adjust the desired temperature. Although this amount of microwave power was sent to the system, only in the range of 10 to 40 W was absorbed by the catalyst resulted in a change in tem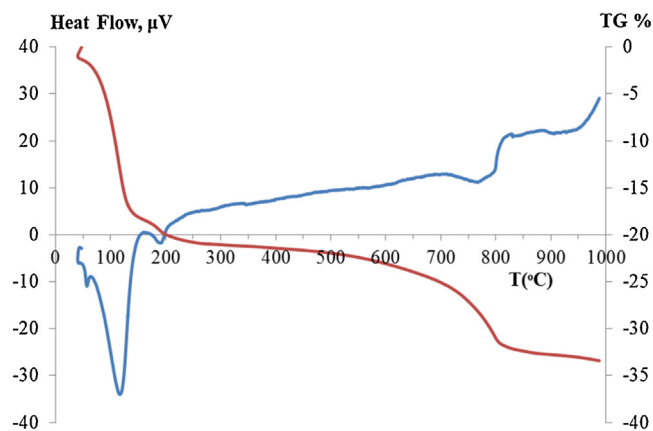perature and the rest of microwave was absorbed by the cooling water. The synthesized catalysts was heated to the similar temperatures using microwave energy possessing a same power up to a temperature value of 500 °C. After this point, it was observed that absorbed amount power by the catalysts changed in the range of 20–40 W for catalysts prepared at different Fe loading. In the microwave reactor system, temperature was increased to the desired value (for instance to 300 °C) within one minute. The MW leakage detector, which was supplied by SAIREM Company, was used to ensure safe working environment during experiments. In both of the systems, high purity gaseous ammonia (99.95%) was fed to the system at a flow rate of 60 ml/min (Q_o), which was adjusted by a mass flow controller. Online analysis of reactant and products was done by a Gas Chromatograph, equipped with Thermal Conductivity Detector (TCD) operated at 180 °C with a 1.5 m long column packed with Porapak Q. Gas outlet composition was determined keeping this column at 30 °C for 15 min interval and Argon was used as the carrier gas at 17 psi. Activity of mesoporous carbon at different reaction temperatures and the stability of catalysts for longer reaction times were tested. Conversion of ammonia (X) to hydrogen was evaluated basing on the data taken form the effluent stream provided by gas chromatograph and calculated using Eq. (1) with the contribution of nitrogen mass balance (Eq. (2)). In these expressions F_{NH3}^0 referred to total amount of ammonia before the reaction, calculated from nitrogen mass balance, F_{NH3} and F_{N2} referred to unconverted amount of ammonia and produced amount of nitrogen, respectively, these were the data provided by the Gas Chromatograph. After reaching steady state at the desired temperature value, at least four successive measurements were carried out and conversion profiles were built using average of them. Conversion values evaluated in these repeated runs were all within ±5% error limits.

$$X = \frac{F_{NH3}^0 - F_{NH3}}{F_{NH3}^0} \times 100 \qquad (1)$$

$$F_{NH3}^0 = F_{NH3} + 2F_{N2} \qquad (2)$$

3. Results and discussion

3.1. Catalyst characterization results

The TGA-DTA curves of uncalcined form of iron incorporated mesoporous carbon catalyst having 10 wt% of iron loading are presented in Fig. 2. Two endothermic peaks, at 115 °C and at 198 °C, were observed in the DTA analysis of the sample. The corresponding weight loss for the former peak was approximately 17% and the corresponding weight loss for the latter one was 3% in TG analysis of the sample. The first weight loss occurred due to hydrated
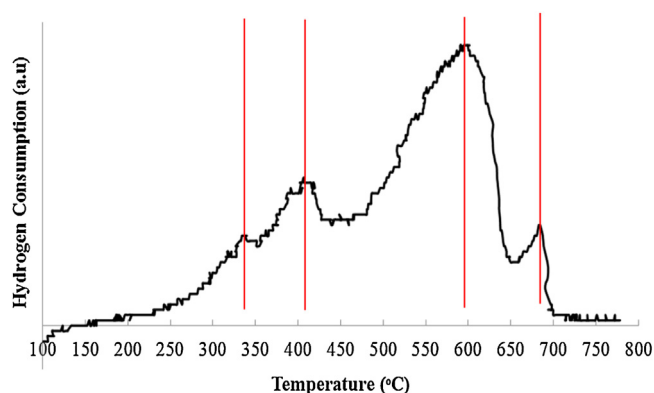
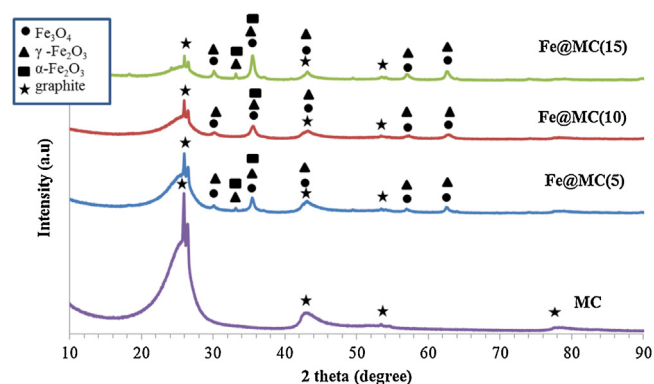**Fig. 3.** TPR result of iron incorporated mesoporous carbon catalyst.

Fig. 4. XRD results of iron incorporated mesoporous carbon catalysts at different metal loadings in their calcined form.

water removal and the latter one could be due to the decomposition of precursor [41]. There was only 2 wt% variation in the weight losses observed between 200 and 600 °C. Considering this figure, synthesized catalysts were calcined at 450 °C, under the flow of pure nitrogen, differently from some studies in literature, which were mentioned the utilization of the static air [40] or the flowing air [37]. Iron nitrate was expected to be decomposed to iron oxides after the calcination of iron incorporated mesoporous catalysts under inert atmosphere [37,38,42] and XRD results of calcined catalysts presented in Fig. 4. supported the formation of iron oxides.

TPR profile of the iron incorporated mesoporous carbon catalyst, prepared with a 10 wt% iron loading, is presented in Fig. 3. It is known that, during the reduction of iron based catalysts, firstly, phase transformation of Fe_2O_3 to Fe_3O_4 takes place, then Fe_3O_4 converts to FeO and finally transformation of FeO to metallic iron occurs [42–45,40]. Therefore, the first peak, observed at 339 °C, was related to the reduction of Fe_2O_3 to Fe_3O_4. For this transformation, temperature values in the range of 300 °C [44] to 350 °C [43] were reported in the literature. Xiong et al. [45] synthesized Fe/CNT catalysts and they mentioned that Fe_2O_3 particles located inside the CNT were reduced at 301 °C, while Fe_2O_3 particles located outside wall of the CNT were reduced at higher temperatures (339 °C). So, it could be expected that larger fraction of iron oxides, in the present study, were possibly located outside of the pores rather than inside of the pores. This statement is supported by the nitrogen adsorption desorption analysis presented in Figs. 7 and 8 and Table 1. The second peak, which was seen at 405 °C, corresponded to the reduction of Fe_3O_4 to FeO. As supported by Xiong et al. [45], higher amount of hydrogen was required to reduce Fe_3O_4 than to reduce Fe_2O_3. Xiong et al. [45] reported that this reduction should take place at 435 °C, while a reduction temperature of 450 °C was reported by Lorenzut et al. [44]. The third peak, which was seen

at 595 °C, was associated to the reduction of FeO to metallic Fe. Xiong and coworkers [45] indicated that this reduction occurred in a temperature interval of 475–600 °C and it required much higher amount of hydrogen than that of the formers. Indeed, Lorenzut et al. [44] and Liao et al. [43] mentioned much higher temperatures that were over 600 °C, for the formation of metallic iron. In the work of Chen et al. [46], it was mentioned that reactions of iron oxides during the reduction of iron ore were classified into two types, namely direct and indirect reduction. In the direct reduction, iron (Fe) could be formed as a result of reaction between solid carbon and iron oxides (FeO) at temperatures higher than 950 °C. So, in the present study direct reduction is not supposed to be occurred. In the case of indirect reduction, either CO or H_2 was used and it took place at temperatures lower than 900 °C. Chen et al. [46] reported that in the H_2-based indirect reduction processes, reduction of Fe_3O_4 was governed by the formation of metallic iron (Fe) or FeO. Both of the reactions were endothermic, but formation of Fe was governed by the reaction of 4 mol of H_2 per mol of Fe_3O_4 at temperatures lower than 570 °C. On the other hand, formation of iron oxide was seen with the reaction of 1 mol of H_2 per 1 mol of Fe_3O_4 at temperatures over 570 °C, than it was further reduced to metallic iron. According to this statement, metallic iron crystallites could be observed in the structure of iron incorporated mesoporous catalysts after their reduction at 500 °C under the flow of pure hydrogen. The last peak seen in Fig. 3 is related to the methanation reaction of carbon support in the presence of hydrogen, at high temperatures to produce methane [45].

X-ray diffraction patterns of the synthesized catalysts, in their calcined form, are presented in Fig. 4. XRD of pure mesoporous carbon (MC) is also seen in the same figure. It has high intensity peaks at 2θ values of 25.9, 26.4, 42.7°, with the lower intensity peaks observed at 2θ values of 53.56 and 78.22°. These peaks indicate graphite-like carbon structure within the catalysts, according to JCPDS card 00-041-1487 and they are still present in the structure of iron incorporated catalysts having different metal loadings. Graphite like structure is supposed to be important in the evaluation of the dielectric properties of mesoporous carbon. In a very detailed work of Du et al. [47], microwave absorption properties of ordered mesoporous carbon, disordered mesoporous carbon and nonporous carbon materials were investigated. They reported the degree of graphitization as being the primary factor affecting the microwave absorbing properties of carbon materials and mesoporous carbon having suitable degree of graphitization and uniform pore structure could be used as excellent microwave absorbers. Peaks observed at 2θ values of 30.0, 33.1, 35.4, 49.1, 57.0 and 62.5° in the X-ray diffraction patterns of Fe@MC(5) catalyst indicated the presence of iron oxides in the catalyst structure. According to JCPDS card No.00-039-1346, diffraction peaks observed at 2θ values of 30.24° (220), 33.88° (310), 35.63° (311), with d spacing values of 0.2953, 0.2644 and 0.2518 nm, respectively, belong to maghemite (γ –Fe_2O_3). Peaks observed at 2θ values of 43, 54, 57 and 63° correspond to (400), (422), (511) and (440) planes of maghemite structure, respectively. Peak, which was supposed to be at 43°, appeared at the same location with the main diffraction line of graphite carbon. Meanwhile, peaks at 2θ values of 30.0, 35.4, 57.0 and 62.5° correspond to the crystal planes of magnetite (Fe_3O_4), considering the JCPDS card No.01-076-0955. Moreover, peaks observed at 2θ values of 32.6° and 38.5° were the (104) and (110) diffraction planes of crystalline hematite α-Fe_2O_3 phase, respectively, according to ICDD card 73-0603 [40]. So the iron oxides, namely maghemite, magnetite and hematite, appeared simultaneously in the structure of iron incorporated mesoporous carbon catalysts. In the work of Sinovski et al. [48], it was indicated that 2θ values of 35.4°, 43.0° and 62.5° correspond to (311), (400) and (440) crystal plane of iron oxides (Fe_3O_4 and γ-Fe_2O_3). They mentioned that the structures of Fe_3O_4 and γ-Fe_2O_3 were very

Table 1
Physical Properties of Synthesized Catalysts.

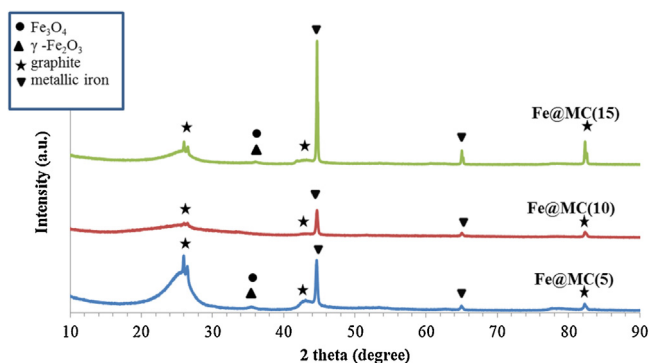| Catalyst	Multipoint BET Surface Area (m^2/g)	BJH desorption Surface Area (m^2/g)	BJH desorption Pore Volume (cc/g)	BJH desorption Pore Diameter (nm)
MC	217	262	0.50	6.59
Fe@MC(5)	226	257	0.48	7.85
Fe@MC(10)	231	262	0.42	3.41
Fe@MC(15)	207	207	0.31	4.27
Fe@MC(10)M	223	265	0.56	7.76
Fe@MC(10)C	227	262	0.46	7.79

Fig. 5. XRD results of iron incorporated mesoporous carbon catalysts at different metal loadings in their reduced form.

Fig. 6. HRTEM images of mesoporous carbon (a), Fe@MC(10) in reduced form (b).

similar to each other so it was difficult to distinguish each one of them according to their XRD pattern or FFT images. They proposed that it might be assumed that either one or both of the iron oxides could be present in the same sample. Cruz et al. [40] also indicated the presence of α-Fe$_2$O$_3$ simultaneously with γ-Fe$_2$O$_3$ and Fe$_3$O$_4$ in the polymeric mesoporous carbon supported iron based catalysts by Mössbauer Spectroscopy. Xiong et al. [45] reported that, the peak observed at 2θ value of $35.5°$ was the sign of the presence of both forms of iron oxide phases. Duan et al. [39] reported that calcination temperature for iron incorporated ordered mesoporous carbon catalyst was important for the crystallinity of iron oxides. In this study, formation of Fe$_3$O$_4$ and γ-Fe$_2$O$_3$ was observed for the samples prepared by iron nitrate and calcined at $450°C$ under nitrogen flow, as indicated in the experimental part. Formation of maghemite, magnetite and hematite were also seen at higher metal loadings (Fig. 4). The size of iron oxide crystals were calculated using Scherrer equation from the line broadening of the (311) plane of iron oxides, as accepted by the literature, and found as 18.9 nm, 11.2 nm and 16.8 nm for Fe@MC(5), Fe@MC(10) and Fe@MC(15) catalysts, respectively.

X-ray diffraction patterns of the reduced catalysts are presented in Fig. 5. Peaks corresponding to the iron oxides are in very low intensities in the structure of Fe@MC(5) and Fe@MC(15) catalysts, while they could not be observed in the structure of Fe@MC(10). On the other hand, peaks beloging to the metallic iron are clearly seen for all of the catalysts, at 2θ values of $44.6°$ (110) and $65°$ (200). Unlike the TPR results given in Fig. 3, XRD analyses showed that, formation of metallic iron could be achieved at a reduction temperature of $500°C$, which was supported by the literature [46,48]. As discussed previously, Chen et al. [46] mentioned the formation of metallic iron with the H$_2$-based indirect reduction of iron oxides at temperatures lower than $570°C$ and Sinovski et al. [48] also observed the elemental iron after hydrogen reduction of iron oxides (Fe$_3$O$_4$ and Fe$_2$O$_3$) at $450°C$. As indicated in the experimental part of this manuscript, catalysts were reduced at $500°C$, under the flow of pure hydrogen. The size of metallic iron was calculated using Scherrer equation, from the line broadening of the (110) diffrac-

tion peak and found as 29.6 nm, 29.6 nm and 51.8 nm for Fe@MC(5), Fe@MC(10) and Fe@MC(15) catalyst, respectively.

HRTEM images of pure mesoporous carbon, (Fig. 6a), and iron incorporated mesoporous carbon in reduced form, (Fig. 6b) supported that the structure of carbon did not collapse after the impregnation of metal. This was also seen in the XRD analyses presented in Fig. 4. As indicated in the experimental part, catalysts were prepared changing the weight percent of iron in the synthesis solution from 5 to 15 wt% and ICP-OES results of Fe@MC(5), Fe@MC(10) and Fe@MC(15) gave 3.4, 7.7 and 12.9 wt% of Fe, respectively. According to these results, metal loading was achieved without destroying the structure of the support. Metallic iron crystals in cubic form, can be clearly seen in HRTEM image of reduced Fe@MC(10) catalyst (Fig. 6b). The particle size of metallic iron observed in HRTEM image is around 10 nm, which is smaller than the crystal size obtained from XRD results.

Nitrogen adsorption/desorption isotherms of the calcined catalysts having different metal loadings are presented in Fig. 7, together with the isotherms of mesoporous carbon. As seen in this figure, mesoporous carbon has Type IV isotherm with type H2 hysteresis loop, according to IUPAC classification. This type of hys-
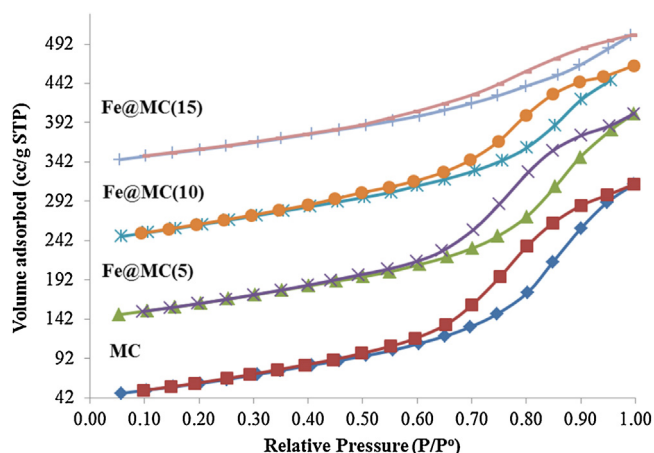
Fig. 7. Nitrogen/adsorption desorption isotherms of iron incorporated mesoporous carbon catalysts in their calcined form.
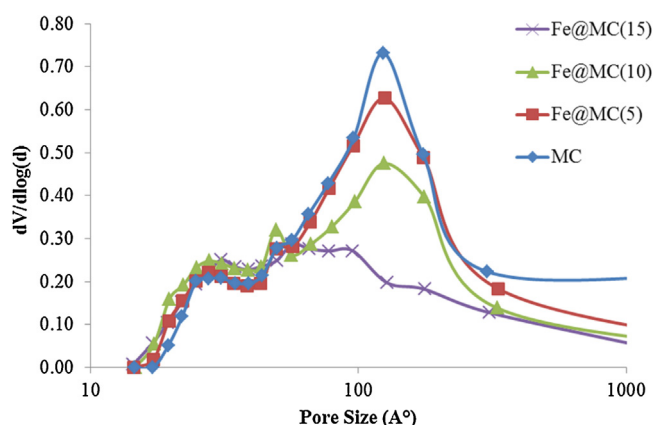

Fig. 8. Pore size distribution of iron incorporated mesoporous carbon catalysts in their calcined form.

Fig. 9. Results of conventional system experiments (GHSV$_{NH3}$: 36000 ml/h g$_{cat}$).
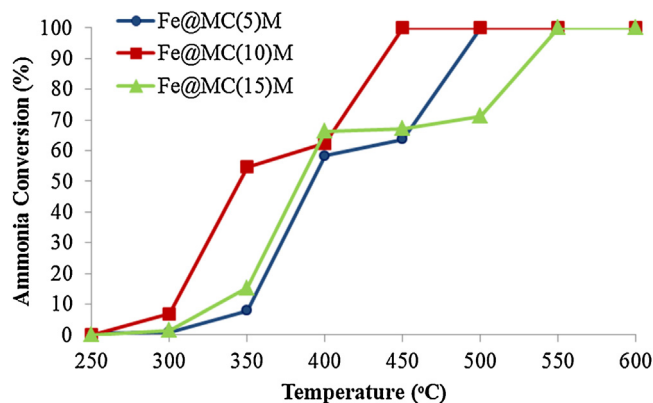
Fig. 10. Results of microwave system experiments (GHSV$_{NH3}$: 36000 ml/h g$_{cat}$).

teresis loop is explained with the Network Model that could be due to interconnected porous network [49]. HRTEM image of mesoporous carbon presented in Fig. 6a also supported this ordered structure. Impregnation of iron did not change the type of the isotherms however it affected the surface area and the pore volume of the catalysts, especially at the highest metal loading. The pore size distribution of mesoporous carbon was plotted using adsorption branch of isotherms (Fig. 8) and bimodal porosity having peak positions at around 2.8 nm and 12.4 nm, was observed. Obtaining similar trend in the pore size distribution plotted using desorption branch of isotherms supports the dual model porosity [50]. Metal loading decreases the pore volume of the catalysts and it is possibly attributed to a blocking of pores in the mesoporous range by iron oxides. As the metal loading increases, the decrease in surface area and pore volume become clearly seen (Table 1). It is worth to note that nitrogen adsorption/desorption analyses were applied to the reduced form of the catalysts as well and very similar results were revealed such that BJH desorption surface area of Fe@MC(5) catalyst in reduced form was 255.6 m^2/g and the corresponding values for pore volume and pore diameter were 0.46 cc/g and 7.83 nm, respectively.

3.2. Catalytic activity results

Results of ammonia decomposition reaction over iron incorporated mesoporous carbon catalysts in conventional reactor system and microwave reactor system are presented in Figs. 9 and 10,
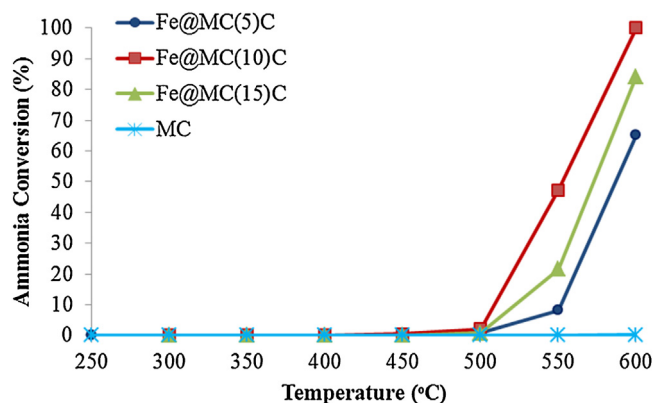
respectively. In this part, Fe@MC(X)C referred to Fe@MC(X) catalysts tested in Conventional System and Fe@MC(X)M referred to the catalysts studied in Microwave System. For both of the systems, GHSV of ammonia was adjusted to 36000 ml/h g$_{cat}$.

It was clearly seen that negligible amount of product was formed in the Conventional System; when the reaction temperature was lower than 500 °C. Increase in reaction temperature over this value caused an increase in the activity of the catalysts. For example, 8% ammonia conversion was obtained over Fe@MC(5) and 47% ammonia conversion was achieved over Fe@MC(10) at the reaction temperature of 550 °C. Although Fe@MC(15) catalyst had the highest metal loading, it only showed 21% ammonia conversion at the same temperature. The lower activity of Fe@MC(15) compared to that of Fe@MC(10) could be explained with the lower surface area and larger metallic iron crystals formed in the structure of the former one. When the reaction temperature was 600 °C, ammonia conversion values over 65% were obtained in the Conventional System and the maximum conversion was achieved with Fe@MC(10) among all the synthesized iron incorporated mesoporous carbon catalysts. Activity of pure mesoporous carbon in ammonia decomposition reaction was also investigated in conventional reactor system and negligible conversion values were obtained even at the highest reaction temperature, as seen in Fig. 9. So it can be certainly said that iron incorporation to the mesoporous carbon enhanced the activity significantly. The lowest activity of Fe@MC(5) during conventional heating could be revealed that increasing metal loading could be resulted in a better performance during reaction. However, it should be pointed out that size and distributions of active sites have a great contribution to the activity of the catalysts, as indicated previously.

In the focused Microwave System, negligible activity was obtained below 250 °C, which was not presented here. When the reaction temperature was 300 °C, 7% ammonia conversion was seen over Fe@MC(10) unlike the other ones. As depicted from Fig. 10, all of the synthesized catalysts showed activity at 350 °C. While ammonia conversion values in the range of 7–15% were obtained over Fe@MC(5) and Fe@MC(15), 55% conversion was achieved over Fe@MC(10) at this temperature. Ammonia conversion values higher than 58% could be seen at 400 °C in the focused microwave system. By increasing the reaction temperature to 450 °C, overall conversion value was reached using Fe@MC(10). As seen in Fig. 10, variation in the conversion values was not changing significantly between 350 and 400 °C, seems like a shoulder, for Fe@MC(10) catalyst. The same behavior was also seen in the conversion profiles of Fe@MC(5) and Fe@MC(15) starting from 400 °C. In Microwave System temperature adjustments were carried out by changing the power of the microwave generator throughout the reaction. For all the experiments, initially generator power was set to 0.06 kW and it was gradually increased to 0.09 kW to obtain higher temperatures. Although this amount of microwave power was sent to the system, maximum amount of microwave absorbance was recorded about 40 W. For controlling temperature value especially lower that 450 °C, microwave power about 10 W was even sufficient. Therefore, changes occurred in the microwave power could be possible reason of the formation of these shoulders in conversion values. Moreover, some electrical arcs or namely hot spots which were experimentally observed at high temperatures during the reaction could be the explanation of a rapid increase in the conversion after these shoulders. For both of the reactor systems, Fe@MC(10) showed the highest activity among the synthesized catalysts. It is known that size and distribution of the active particles formed in the catalyst structure could be greatly effective on the variation of the activities. As supported by XRD and HRTEM results, reduced form of this catalyst had only metallic iron crystallites having the size of 10 nm and these were smaller than the crystallites observed in the structure of the other ones. Lanzani et al. [51] reported that rate of ammonia decomposition was influenced by the size of iron particles and smaller ones exhibited higher activities. So, the highest activity of Fe@MC(10) could be explained with the small iron particles formed in its structure.

Results presented in Figs. 9 and 10 indicated that a comparable ammonia conversion values were obtained with Microwave System for each of the catalyst. Unlike the Conventional System, at which electrical furnace was used to supply necessary heat, conversion of ammonia could be started just above 250 °C. All the synthesized catalysts showed activity at 350 °C, reaching to 55%, which was not possible in Conventional System. When the reaction temperature was increased to 400 °C, the difference in catalytic performance of catalysts in these two systems was over 60%. For example Fe@MC(15) gave 66% ammonia conversion in Microwave System while it did not show any activity in Conventional System. While the activity of catalysts were negligible up to 500 °C in Conventional System, overall conversion was reached at 500 °C, 450 °C and 550 °C using Fe@MC(5), Fe@MC(10) and Fe@MC(15), respectively, in Microwave System.

These observations could be explained with the differences occurred in heating mechanisms of the conventional system and the microwave system. In the case of conventional heating, heat is transferred firstly to the walls and the cavity of the furnace than it is transferred to the sample, by means of convection and conduction mechanisms. Therefore a decrease in temperature can be observed in radial direction for such an endothermic reaction, as seen in the work of Durka et al. [52] who investigated experimentally the temperature distribution throughout a catalytic bed that was used for methanol steam reforming reaction. Their reactor having dimensions of 24 mm OD and 12 mm in height, was heated from the bottom with the help of electrical heating and results showed that temperature near the wall was higher than temperature at the core due to these heat transfer mechanisms. In the case of microwave heating, energy conversion occurs i.e., microwave energy is transferred to catalysts and heat is generated where it is needed and heat losses due to the heating of the walls and cavity are avoided [24,23]. So, higher conversion values could be achieved in reaction system that was also supported by the literature for example, Durka et al. [52] reported that higher methanol conversion values, over 10%, were achieved at the same temperature using the same reactor under microwave heating in comparison to conventional heating.

In the literature, it was indicated that inverse temperature profile could be occurred due to volumetric heating in microwave system that resulted in higher conversion values, as well. In the study of Durka et al. [52], lower part of the reactor that contained the catalytic bed was exposed to microwave and temperature gradients in axial and radial direction were observed. Their results showed that temperature of the core was found to be higher than the temperature near the wall due to volumetric heating. Formation of inverse temperature profile that resulted in formation of the hottest area in the middle of the catalytic bed was also discussed by Krech et al. [53]. This would be effective obtaining higher conversion values in microwave used system.

As indicated previously, under microwave heating, hot spots, which can be seen as electric arcs, may also formed within the bed, and their temperatures are expected to be higher than the overall bed temperature. In the literature it was indicated that the difference observed in the microwave absorption ability of metal/-oxides crystals and the support materials caused hot spot formation [52]. These hot spots are also considered as "microplasmas" and their higher local (microscale) temperatures comparing to the average bulk temperature are supposed to increase the conversion [27,31,52], as well. Durka et al. [54] mentioned that infrared pyrometers measured the surface temperature and surface temperature could be close to the bulk temperature if very thin samples were used. Moreover, measurements of microscopic scale hot spots could not be carried out since infrared pyrometers measured the macroscale temperatures. During the experiments, some randomly formed electrical arcs were observed especially at temperatures above 500 °C, however, their temperatures could not be measured by infrared pyrometer. Therefore, one of the possible reason of higher conversion that was achieved under microwave heating could be the formation of hot spots, as supported by the literature.

Furthermore, Fidalgo et al. [30] mentioned the enhanced affect of N_2 present in reactor on the formation of more energetic microplasmas i.e. hot spots of higher temperature. During the ammonia decomposition reaction, nitrogen was also produced and it might also enhance the reaction.

Studies on the good microwave absorption properties of iron based nanostructured materials such as Fe, γ-Fe_2O_3, Fe_3O_4 considering their morphology and structural properties have been found in the literature [55]. Besides, Fe particles surrounded by some carbon materials were also investigated and microwave absorption properties of this kind of materials were found to be very high [56–58]. Excellent microwave absorption characteristics of CNT/crystalline Fe nanocomposites [56], α-Fe_2O_3/ordered mesoporous carbon nanocomposites were reported [59]. Yuan et al. [58] mentioned that excellent microwave properties of mesoporous carbon coated magnetite particles were due to the contribution of each component. Therefore, higher activity of iron incorporated mesoporous catalyst in microwave system could also be explained with the expected good absorption properties of these catalysts.

In order to investigate the catalyst stability and reliability of microwave reactor, a set of time-on stream reaction tests, was performed using in this system. Experiments were carried out using
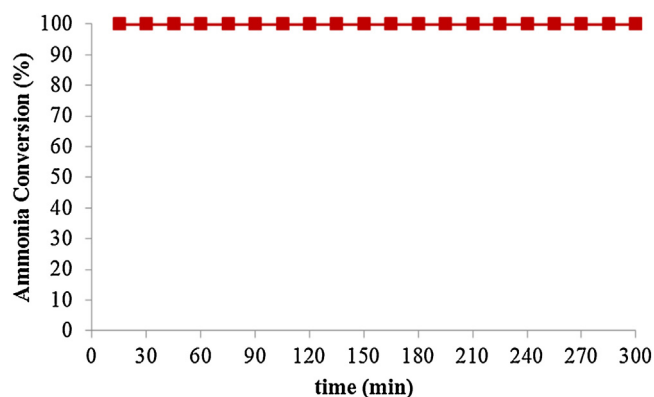
Fig. 11. Stability test of Fe@MC(10) at 450 °C (GHSV$_{NH3}$: 36,000 ml/h g$_{cat}$).

Fe@MC(10) catalyst which gave the highest activity among the synthesized catalysts. Reaction temperature was set to 450 °C at which overall conversion was achieved. As seen in Fig. 11, ammonia conversion value was highly stable during the reaction period.

Commonly carbon nanotubes were used as support material for iron precursors or iron nanoparticles and the synthesized catalysts were tested in ammonia decomposition reaction in a conventionally heated reactor (Table 2). For example, Zhang and coworkers [9] used commercial carbon nanotubes, which had contained 2.8 wt% of iron nanoparticles, and they reported 76% conversion of ammonia at 700 °C at a space velocity of 5000 ml/h g$_{cat}$. [9]. Duan and coworkers [16] tested Fe supported on carbon nanofiber catalysts having 3.5 wt% Fe at a GHSV of 6500 ml/h g$_{cat}$. Ammonia conversion of 51.3% was reported at 600 °C [16]. Application of ordered mesoporous carbon in the preparation of iron catalysts to be used in ammonia decomposition was recognized in the work of Lu and coworkers [15] to the best of our knowledge. They prepared catalysts by impregnating aqueous solution of iron nitrate on CMK-5 which was a bimodal mesoporous ordered carbon. In this very detailed study, Lu et al. [15] reported a complete conversion of ammonia over γ-Fe$_2$O$_3$/CMK-5 catalysts at 600 °C with a space velocity of 7500 cm^3/h g$_{cat}$. They also carried out experiments at a higher space velocity such as 60000 cm^3/h g$_{cat}$ and they reported total conversion at 700 °C under this condition. In the present study, total conversion was achieved over Fe@MC(10) catalyst, i.e. nominal Fe loading was 7.7 wt%, at 600 °C with GHSV of 36000 ml/h g$_{cat}$ when the reactions were carried out in conventionally heated system. This result is better than the given values for iron incorporated carbon catalyst in ammonia decomposition reaction. When the reaction was carried out in Microwave System using Fe@MC(10) at GHSV of 36000 ml/h g$_{cat}$, total conversion was achieved, even at 450 °C, as presented in Fig. 10. This is the best reported catalytic activity for iron incorporated carbon supported catalyst in ammonia decomposition. It is known that ruthenium is the most active metal to produce hydrogen from ammonia and Li and coworkers [60] used different carbon supports such as mesoporous carbon (CMK-3), carbon nanotubes, activated carbon, carbon black and graphite carbon for ruthenium. Catalysts having a nominal metal loading of 5% were prepared by impregnation procedure and tested in conventionally heated system. Results of experiments carried out at 550 °C with pure ammonia (GHSV of 30000 ml/h g$_{cat}$) revealed that 14.4, 22.7, 52.7, 84.7 and 95.0% ammonia conversion for activated carbon, mesoporous carbon, carbon black, carbon nanotube, graphite carbon supported ruthenium catalysts, respectively. Activity of mesoporous carbon supported catalysts prepared at 10–15 wt% loading was comparable even higher than the activity of mesoporous carbon supported Ru catalyst worked by Li and coworkers [60]. The improved activity of catalysts by using Microwave System was clearly seen that
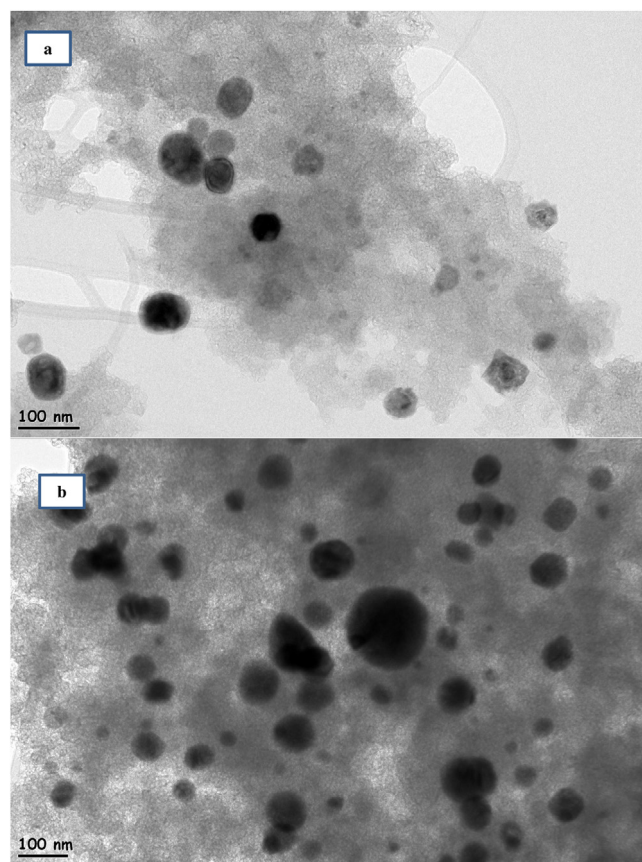

Fig. 12. HRTEM images of (a) Fe@MC(10)C and (b) Fe@MC(10)M.

Fe@MC(10) catalyst showed better activity than graphite carbon supported Ru catalyst which was the most active one with 95% conversion value.

3.3. Characterization of used catalysts

Characterization tests, namely XRD, nitrogen adsorption/desorption and HRTEM analyses were also applied to the used catalysts to see any changes in their structure. Fe@MC(10) catalyst showed the highest activity in both of the systems. In the HRTEM images of Fe@MC(10)C and Fe@MC(10)M, presented in Fig. 12, some particles were observed and their EDX analyses indicated that they were containing iron and carbon elements. In order to determine whether these were metallic iron or any compound that were formed between iron and carbon, X-ray diffraction patterns of spent catalysts for both systems were investigated (Fig. 13). Metallic iron crystals were determined in the reduced form of iron incorporated mesoporous catalysts, as indicated in Fig. 5. When the catalysts were used in the conventional system, metallic iron crystals were still present and their crystal sizes, which were calculated using Scherrer equation from the line broadening of the (110) plane, were 27.7, 31.9 and 41.6 nm, for Fe@MC(5)C, Fe@MC(10)C, Fe@MC(15)C, respectively. Peaks corresponding to graphite structure were also observed in the structure of catalysts being used in the conventional system. In the X-ray diffraction patterns of the catalysts that were used in the microwave system, peaks corresponding to the metallic iron could not be seen. On the other hand, new peaks were observed at 2θ values between 40 and 47°. These four peaks corresponded to the iron carbide structure (Fe$_5$C$_2$), considering the JCPDS card No.00-020-0508. It is known that, carbides of different transition metals such as vanadium, molybdenium have been considered for ammonia decomposition

Table 2
Catalytic Activities of Different Catalyst for Ammonia Decomposition Reaction.

Catalyst	Metal Content (wt%)	T (°C)	GHSV (ml/g$_{cat}$ h)	NH3 conversion (%)	Ref.
Fe containing CNT	2.8	700	5000	75.1	[9]
Fe/CNFs	3.5	600	6500	51.3	[16]
γ-Fe$_2$O$_3$/CMK-5	5.2	600	7500	98	[15]
Mesoporous Fe$_3$C		700	15000	95	[62]
Fe$_3$C on AC		700	5000	60	[9]
Ru@Graphite Carbon	5	550	30000	95	[60]
Fe@MC(10)C	7.7	600	36000	complete	present
Fe@MC(10)M	7.7	450	36000	complete	present

Fig. 13. XRD results of the iron incorporated mesoporous carbon catalyst in their used form.

Fig. 14. Nitrogen adsorption/desorption isotherms of the iron incorporated mesoporous carbon catalyst in their used form.

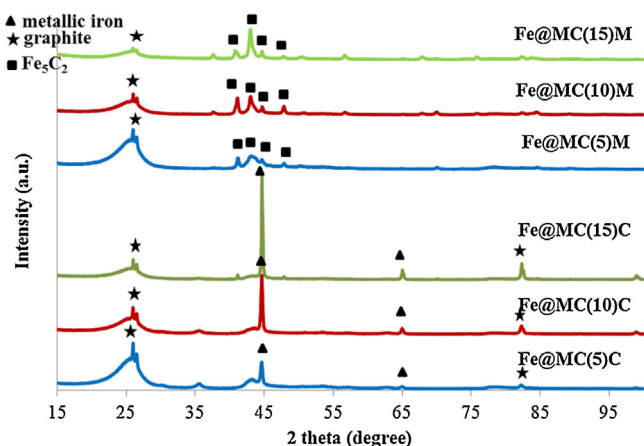**Fig. 15.** Pore size distribution of the iron incorporated mesoporous carbon catalyst in their used form.

reaction [61–63]. In the work of Kraupner et al. [62], catalytic activities of iron carbide in ammonia decomposition reaction at a GHSV of 15000 cm^3/g$_{cat}$ h were studied and 20% ammonia conversion value was reported at a reaction temperature of 550 °C. An increase in reaction temperature enhanced the reaction and 95% ammonia conversion was reported at 700 °C under the same feed flow rate. Previoulsy in the work of Zhang et al. [9], Fe carbide supported on activated carbon were utilized in ammonia decomposition reaction (GHSV: 5000 ml/g$_{cat}$ h) and conversion values gradually increased and approached to steady state with a value of 60% at 700 °C. Under the same conditions, 2.8 wt% Fe containing carbon nanotube catalyst show 75% ammonia conversion. These studies revealed that iron carbides were also active in ammonia decomposition reaction as well as metallic iron. Considering the activity of catalysts on ammonia decomposition reaction in microwave system (Figs. 10–11), it can be said that formation of iron carbide may also contribute to the higher performance of this catalyst.

As indicated previously, among the synthesized iron incorporated mesoporous carbon catalysts, Fe@MC(10) showed the highest activity in both reactor systems.The nitrogen adsorption/desorption isotherms of this catalyst and its used forms, namely Fe@MC(10)M and Fe@MC(10)C, are presented in Fig. 14. Similar isotherms and pore size distribution curves (Fig. 15) were obtained for both Fe@MC(10)C and Fe@MC(10)M. After being used in either the conventional system or microwave system, surface area of Fe@MC(10) catalyst did not change, as seen in Table 1. However, an increase in pore diameter as well as pore volume was clearly seen after their utilization. While the pore volume of Fe@MC(10) was 0.42 cc/g, it became to 0.46 cc/g and 0.56 cc/g, after being used in conventional and microwave system, respectively. Moreover, average pore diameter of Fe@MC(10) increased from 3.41 nm to 7.8 nm after being used in reaction. These results show that variation in surface area and the properties of pores changed in a similar manner in both systems so that microwave energy did not
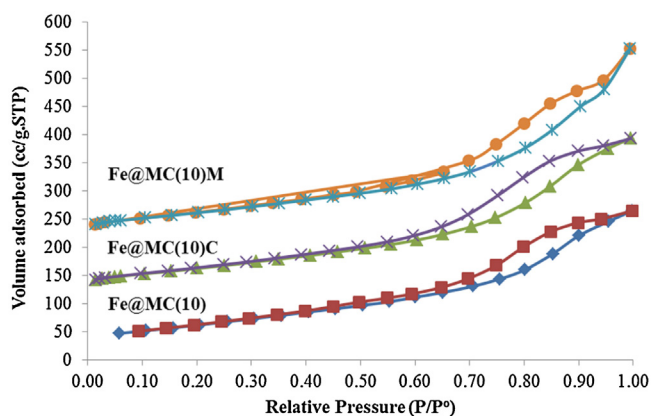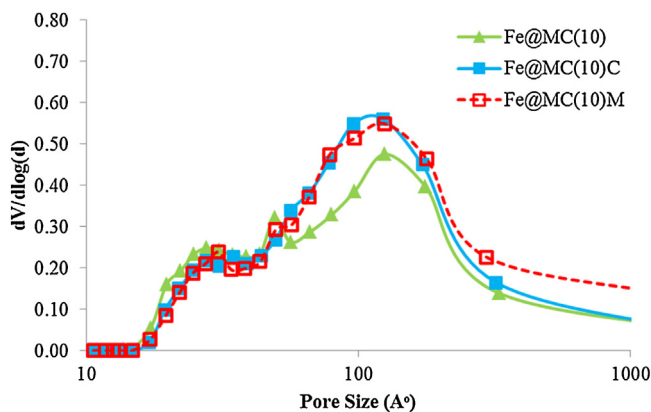
affect the pore structure of the iron incorporated mesoporous catalysts, which was supported by the HRTEM images of Fe@MC(10)C and Fe@MC(10)M (Fig. 16). Moreover, possibility of catalyst sintering due to microwave application to the catalyst structure could not be expected, considering the results presented in Figs. 12–16.

4. Conclusions

Microwave-assisted ammonia decomposition reaction was investigated using iron incorporated mesoporous carbon catalysts prepared by impregnation procedure. When the performances of the synthesized catalysts were evaluated in the Conventional System with a GHSV of 36000 ml/h g$_{cat}$, negligible activity was observed below 500 °C. With an increase in reaction temperature, conversion was increased and complete conversion was achieved at 600 °C. In the case of Microwave System, conversion of ammonia was observed at temperatures as low as 300 °C. For all of the
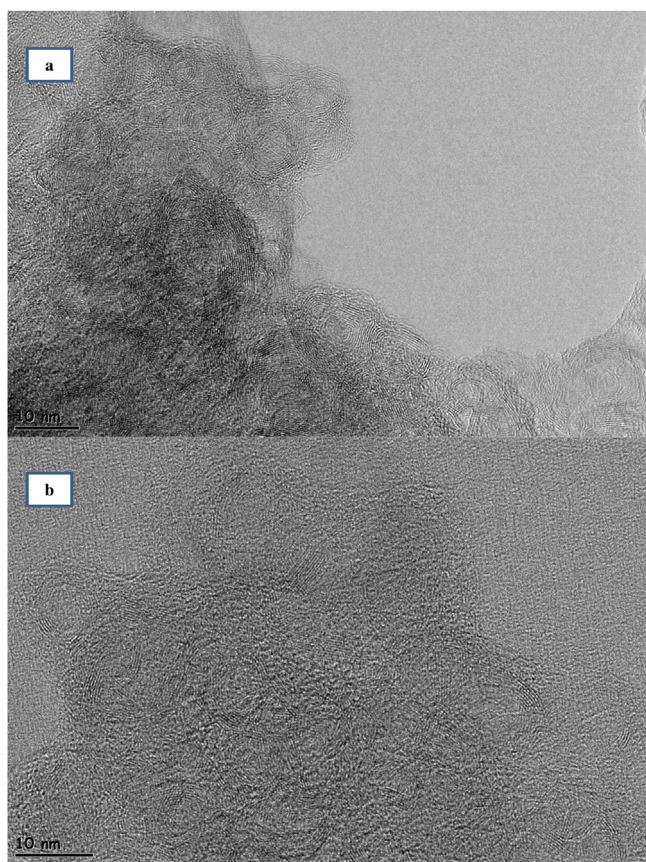
Fig. 16. HRTEM images of A) Fe@MC(10)C and B) Fe@MC(10)M.

synthesized catalysts, conversion values over 60% were obtained at 400 °C. Moreover complete conversion was achieved at 450 °C, over the catalyst, which contained 7.7 wt% Fe, at (with GHSV of 36000 ml/h g_{cat}). Higher activity obtained in the microwave system could be explained with the transfer of microwave energy directly to the catalysts. Formation of hot spots, which were also considered as "microplasmas", within the catalytic bed was considered as another possible reason of an increase in the catalyst activity, as compared to conventionally heated system. Mesoporous carbon which was used as the catalyst support acted as a microwave receptor in the reaction medium. Iron oxides, namely maghemite (γ-Fe$_2$O$_3$), magnetite (Fe$_3$O$_4$) and hematite (α-Fe$_2$O$_3$) appeared simultaneously in the structure of catalysts after calcination at 450 °C under pure N$_2$ flow and they transformed to metallic iron after reduction at 500 °C under pure H$_2$ flow. Formation of iron carbide crystal was observed in the structure of catalysts when they were used in microwave reactor system, while metallic iron was still present in the catalysts when they were tested in conventionally heated system. Therefore formation of iron carbide during microwave heating could be appointed as one the factors leading to a better ammonia conversion.

Acknowledgment

References

[1] T.V. Choudhary, C. Sivadinarayana, D.W. Goodman, Catalytic ammonia decomposition: COx-free hydrogen production for fuel cell applications, Catal. Lett. 72 (2001) 197–201.

[2] X.-K. Li, W.-J. Ji, J. Zhao, S.-J. Wang, C.-T. Au, Ammonia decomposition over Ru and Ni catalysts supported on fumed SiO$_2$ MCM-41, and SBA-15, J. Catal. 236 (2005) 181–189.

[3] M. Reli, N. Ambrozova, M. Sihor, L. Matejová, L. Capek, L. Obalová, Z. Matej, A. Kotarba, K. Kocí, Novel cerium doped titania catalysts for photocatalytic decomposition of ammonia, Appl. Catal. B: Environ. 178 (2015) 108–116.

[4] F. Schüth, R. Palkovits, R. Schlögl, D.S. Su, Ammonia as a possible element in an energy infrastructure: catalysts for ammonia decomposition, Energy Environ. Sci. 5 (2012) 6278–6289.

[5] M.R. Rahimpour, H.R. Mottaghi, M.M. Barmaki, Hydrogen production from urea wastewater using a combination of urea thermal hydrolyser-desorber loop and a hydrogen-permselective membrane reactor, Fuel Process. Technol. 91 (2010) 600–612.

[6] M.R. Rahimpour, M.M. Barmaki, H.R. Mottaghi, A comparative study for simultaneous removal of urea, ammonia and carbon dioxide from industrial wastewater using a thermal hydrolyser, Chem. Eng. J. 164 (2010) 155–167.

[7] C.-M. Hung, Decomposition kinetics of ammonia in gaseous stream by a nanoscale copper-cerium bimetallic catalyst, J. Hazard. Mater. 150 (2008) 53–61.

[8] K. Hashimoto, N. Toukai, Decomposition of ammonia over a catalyst consisting of ruthenium metal and cerium oxides supported on Y-form zeolite, J. Mol. Catal. A: Chem. 161 (2000) 171–178.

[9] J. Zhang, M. Comotti, F. Schüth, R. Schlögl, D.S. Su, Commercial Fe- of Co-containing carbon nanotubes as catalysts for NH$_3$ decomposition, Chem. Commun. (2007) 1916–1918.

[10] K. Nagaoka, T. Eboshi, N. Abe, S. Miyahara, K. Honda, K. Sato, Influence of basic dopants on the activity of Ru/Pr$_6$O$_{11}$ for hydrogen production by ammonia decomposition, Int. J. Hydrogen Energy 39 (2014) 20731–20735.

[11] D. Varisli, E.E. Elverisli, Synthesizing hydrogen from ammonia over Ru incorporated SiO$_2$ type nanocomposite catalysts, Int. J. Hydrogen Energy 39 (2014) 10399–10408.

[12] A.K. Hill, L. Torrente-Murciano, Low temperature H$_2$ production from ammonia using ruthenium-based catalysts: synergetic effect of promoter and support, Appl. Catal. B: Environ. 172–173 (2015) 129–135.

[13] X. Duan, J. Ji, G. Qian, X. Zhou, D. Chen, Recent advances in synthesis of reshaped Fe and Ni particles at the tips of carbon nanofibers and their catalytic applications, Catal. Today 249 (2015) 2–11.

[14] K. Okura, T. Okanishi, H. Muroyama, T. Matsui, K. Eguchi, Promotion effect of rare-earth elements on the catalytic decomposition of ammonia over Ni/Al$_2$O$_3$ catalyst, Appl. Catal. A: Gen. 505 (2015) 77–85.

[15] A.-H. Lu, J.-J. Nitz, M. Comotti, C. Weidenthaler, K. Schlichte, C.W. Lehmann, O. Terasaki, F. Schuth, Spatially and size selective synthesis of Fe-based nanoparticles on ordered mesoporous supports as highly active and stable catalysts for ammonia decomposition, J. Am. Chem. Soc. 132 (2010) 14152–14162.

[16] X. Duan, G. Qian, X. Zhou, Z. Sui, D. Chen, Weikang Yuan, Tuning the size and shape of Fe nanoparticles on carbon nanofibers for catalytic ammonia decomposition, Appl. Catal. B: Environ. 101 (2011) 189–196.

[17] J. Ji, X. Duan, G. Qian, P. Li, X. Zhou, D. Chen, W. Yuan, Fe particles on the tops of carbon nanofibers immobilized on structured carbon microfibers for ammonia decomposition, Catal. Today 216 (2013) 254–260.

[18] D. Varisli, N.G. Kaykac, COx free hydrogen production over cobalt incorporated silicate structured mesoporous catalysts, Appl. Catal. B: Environ. 127 (2012) 389–398.

[19] D. Varisli, N.G. Kaykac, Hydrogen from ammonia over cobalt incorporated silicate structured catalysts prepared using different cobalt salts, Int. J. Hydrogen Energy 41 (2016) 5955–5968.

[20] J.A. Menéndez, A. Arenillas, B. Fidalgo, Y. Fernández, L. Zubizarreta, E.G. Calvo, J.M. Bermúdez, Microwave heating processes involving carbon materials, Fuel Process. Technol. 91 (2010) 1–8.

[21] F. Motasemi, Muhammad T. Afzal, A review on the microwave-assisted pyrolysis technique, Renew. Sustain. Energy Rev. 28 (2013) 317–330.

[22] A. Domínguez, B. Fidalgo, Y. Fernández, J.J. Pis, J.A. Menéndez, Microwave-assisted catalytic decomposition of methane over activated carbon for CO$_2$-free hydrogen production, Int. J. Hydrogen Energy 32 (I) (2007) 4792–4799.

[23] J.M. Bermúdez, D. Beneroso, N. Rey-Raap, A. Arenillas, J.A. Menéndez, Energy consumption estimation in the scaling-up of microwave heating processes, Chem. Eng. Process. 95 (2015) 1–8.

[24] C. Bonnet, L. Estel, A. Ledoux, B. Mazari, A. Louis, Study of the thermal repartition in a microwave reactor: application to the nitrobenzene hydrogenation, Chem. Eng. Process. 43 (2004) 1435–1440.

[25] N. Xiao, H. Luo, W. Wei, Z. Tang, B. Hu, L. Kong, Y. Sun, Microwave-assisted gasification of rice straw pyrolytic biochar promoted by alkali and alkaline earth metals, J. Anal. Appl. Pyrolysis 112 (2015) 173–179.

[26] B. Fidalgo, Y. Fernandez, L. Zubizarreta, A. Arenillas, A. Domınguez, J.J. Pis, J.A. Menendez, Growth of nanofilaments on carbon-based materials from microwave-assisted decomposition of CH$_4$, Appl. Surf. Sci. 254 (A) (2008) 3553–3557.

[27] S. Gündüz, T. Dogu, Hydrogen by steam reforming of ethanol over Co-Mg incorporated novel mesoporous alumina catalysts in tubular and microwave reactors, Appl. Catal. B: Environ. 168–169 (2015) 497–508.
[28] A. Dominguez, J.A. Menendez, Y. Fernandez, J.J. Pis, J.M. Valente Nabais, P.J.M. Carrott, M.M.L. Ribeiro Carrott, Conventional and microwave induced pyrolysis of coffee hulls for the production of a hydrogen rich fuel gas, J. Anal. Appl. Pyrolysis 79 (2007) 128–135.
[29] Y. Li, B. Ye, J. Shen, Z. Tian, L. Wang, L. Zhu, T. Ma, D. Yang, F. Qiu, Optimization of biodiesel production process from soybean oil using the sodium potassium tartrate doped zirconia catalyst under microwave chemical reactor, Bioresour. Technol. 137 (2013) 220–225.
[30] B. Fidalgo, Y. Fernandez, A. Domınguez, J.J. Pis, J.A. Menendez, Microwave-assisted pyrolysis of CH_4/N_2 mixtures over activated carbon, J. Anal. Appl. Pyrolysis 82 (2008) 158–162.
[31] B. Fidalgo, A. Domınguez, J.J. Pis, J.A. Menendez, Microwave-assisted dry reforming of methane, Int. J. Hydrogen Energy 33 (2008) 4337–4344.
[32] W.-H. Chen, B.-J. Lin, Hydrogen production and thermal behavior of methanol autothermal reforming and steam reforming triggered by microwave heating, Int. J. Hydrogen Energy 38 (2013) 9973–9983.
[33] W.-H. Chen, B.-J. Lin, Effect of microwave double absorption on hydrogen generation from methanol steam reforming, Int. J. Hydrogen Energy 35 (2010) 1987–1997.
[34] W.-H. Chen, J.-G. Jheng, A.B. Yu, Hydrogen generation from a catalytic water gas shift reaction under microwave irradiation, Int. J. Hydrogen Energy 33 (2008) 4789–4797.
[35] F. Mushtaq, R. Mat, F.N. Ani, Fuel production from microwave assisted pyrolysis of coal with carbon surfaces, Energy Convers. Manage. 110 (2016) 142–153.
[36] H. Li, X. Li, L. Liu, K. Li, X. Wang, H. Li, Experimental study of microwave-assisted pyrolysis of rice straw for hydrogen production, Int. J. Hydrogen Energy 41 (2016) 2263–2267.
[37] C. Minchev, H. Huwe, T. Tsoncheva, D. Paneva, M. Dimitrov, I. Mitov, M. Froba, Iron oxide modified mesoporous carbons: physicochemical and catalytic study, Microporous Mesoporous Mater. 81 (2005) 333–341.
[38] J. Li, J. Gu, H. Li, Y. Liang, Y. Hao, X. Sun, L. Wang, Synthesis of highly ordered Fe-containing mesoporous carbon materials using soft templating routes, Microporous Mesoporous Mater. 128 (2010) 144–149.
[39] F. Duan, Y. Yang, Y. Li, H. Cao, Y. Wang, Y. Zhang, Heterogeneous Fenton-like degradation of 4-chlorophenol using iron/ordered mesoporous carbon catalyst, J. Environ. Sci. 26 (2014) 1171–1179.
[40] M.G.A. Cruz, M. Bastos-Neto, A.C. Oliveira, J.M. Filho, J.M. Soares, E. Rodriguez-Castelon, F.A.N. Fernandes, On the structural, textural and morphological features of Fe-basedcatalysts supported on polystyrene mesoporous carbon for Fischer-Tropsch synthesis, Appl. Cata. A: Gen. 495 (2015) 72–83.
[41] Z.-Z. Qin, T.-M. Su, Y.-X. Jiang, H.-B. Ji, W.-G. Qin, Preparation of W-modified Fe Mo catalyst and its applications in the selective oxidization of p-xylene to terephthalaldehyde, Chem. Eng. J. 242 (2014) 414–421.
[42] Á. Reyes-Carmona, M.D. Soriano, J.M.L. Nieto, D.J. Jones, J. Jiménez-Jiménez, A. Jiménez-López, E. Rodríguez-Castellón, Iron-containing SBA-15 as catalyst for partial oxidation of hydrogen sulfide, Catal. Today 210 (2013) 117–123.
[43] S.-J. Liao, T. Chen, C.-X. Miao, W.-M. Yang, Z.-K. Xie, Q.-L. Chen, Effect of TiO_2 on the structure and catalytic behavior of iron–potassium oxide catalyst for dehydrogenation of ethylbenzene to styrene, Catal. Commun. 9 (2008) 1817–1821.
[44] B. Lorenzut, T. Montini, M. Bevilacqua, P. Fornasiero, FeMo-based catalysts for H_2 production by NH_3 decomposition, Appl. Catal. B: Environ. 125 (2012) 409–417.
[45] H. Xiong, M.A. Motchelaho, M. Moyo, L.L. Jewell, N.J. Coville, Effect of group I alkali metal promoters on Fe/CNT catalysts in fischer–tropsch synthesis, Fuel 150 (2015) 687–696.
[46] W.-H. Chen, M.-R. Lin, A.B. Yu, S.W. Du, T.-S. Leu, Hydrogen Production from stem reforming of coke oven gas and its utility for indirect reduction of iron oxides in blast furnace, Int. J. Hydrogen Energy 37 (2012) 11748–11758.
[47] Y. Du, T. Liu, B. Yu, H. Gao, P. Xu, J. Wang, X. Wang, X. Han, The electromagnetic properties and microwave absorption of mesoporous carbon, Mater. Chem. Phys. 135 (2012) 884–891.
[48] R. Snovski, J. Grinblat, M.-T. Sougrati, J.-C. Jumas, S. Margel, Synthesis and characterization of iron, iron oxide and iron carbide nanostructures, J. Magn. Magn. Mater. 349 (2014) 35–44.
[49] M. Thommes, R. K€ohn, M. Fr€oba, Characterization of mesoporous solids: pore condensation and sorption hysteresis phenomena in mesoporous molecular sieves, Stud. Surf. Sci. Catal. 142 (2002) 1695–1702.
[50] J.C. Groen, L.A.A. Peffer, J. Perez-Ramirez, Pore size determination in modified micro- and mesoporous materials, pitfalls and limitations in gas adsorption data analysis, Microporous Mesoporous Mater. 60 (2003) 1–7.
[51] G. Lanzani, K. Laasonen, NH_3 adsorption and dissociation on a nanosized iron clusters, Int. J. Hydrogen Energy 35 (2010) 6571–6577.
[52] T. Durka, G.D. Stefanidis, T.V. Gerven, A.I. Stankiewicz, Microwave-activated methanol steam reforming for hydrogen production, Int. J. Hydrogen Energy 36 (2011) 12843–12852.
[53] T. Krech, R. Krippendorf, B. Jäger, M. Präger, P. Scholz, B. Ondruschka, Microwave radiation as a tool for process intensification in exhaustgas treatment, Chem. Eng. Process. 71 (2013) 31–36.
[54] T. Durka, G.D. Stefanidis, T.V. Gerven, A. Stankiewicz, On the accuracy and reproducibility of fiber optic (FO) and infrared (IR) temperature measurements of solid materials in microwave applications, Meas. Sci. Technol. 21 (2010) 045108.
[55] G. Sun, B. Dong, M. Cao, B. Wei, C. Hu, Hierarchical dendrite-Like magnetic materials of Fe_3O_4, ($-Fe_2O_3$, and Fe with high performance of microwave absorption, Chem. Mater. 23 (2011) 1587–1593.
[56] R. Che, L.M. Peng, X. Duan, Q. Chen, X. Liang, Microwave absorption enhancement and complex permittivity and permeability of Fe encapsulated within carbon nanotubes, Adv. Mater. 16 (2004) 401–405.
[57] X. Qi, J. Xu, Q. Hua, W. Zhong, Y. Du, Preparation, electromagnetic and enhanced microwave absorption properties of Fe nanoparticles encapsulated in carbon nanotubes, Mater. Sci. Eng. B 198 (2015) 108–112.
[58] K. Yuan, R. Che, Q. Cao, Z. Sun, Q. Yue, Y. Deng, Designed fabrication and characterization of three-dimensionally ordered arrays of core-shell magnetic mesoporous carbon microspheres, ACS Appl. Mater. Interfaces 7 (2015) 5312–5319.
[59] H.J. Wu, L.D. Wang, Y.M. Wang, S.L. Guo, H. Wu, Flower-like α-Fe_2O_3/ordered mesoporous carbon nanocomposite and its enhanced microwave absorption property, Mater. Res. Innovations 18 (4) (2014) 273–279.
[60] L. Li, Z.H. Zhu, Z.F. Yan, G.Q. Lu, L. Rintoul, Catalytic ammonia decomposition over Ru/carbon catalysts: the importance of the structure of carbon support, Appl. Cata. A: Gen. 320 (2007) 166–172.
[61] J.-G. Choi, Ammonia decomposition over vanadium carbide catalysts, J. Catal. 182 (1999) 104–116.
[62] A. Kraupner, M. Antonietti, R. Palkovits, K. Schlicht, C. Giordano, Mesoporous Fe_3C sponges as magnetic supports and as heterogeneous, J. Mater. Chem. 20 (2010) 6019–6022.
[63] E. Garcia-Bordeje, S. Armenise, L. Roldan, Toward practical application of H_2 generation from ammonia decomposition guided by rational catalysts design, Catal. Rev. 56 (2) (2014) 220–237.